Applied Catalysis B: Environmental 235 (2018) 26–35

Contents lists available at ScienceDirect

Applied Catalysis B: Environmental

journal homepage: www.elsevier.com/locate/apcatb

CO_2 reforming with methane over small-sized Ni@SiO_2 catalysts with unique features of sintering-free and low carbon

Fagen Wang[a,*], Bolin Han[a], Linjia Zhang[a], Leilei Xu[b], Hao Yu[c], Weidong Shi[a,*]

[a] Institute of Green Chemistry and Chemical Technology, School of Chemistry and Chemical Engineering, Jiangsu University, Zhenjiang 212013, China
[b] Collaborative Innovation Center of the Atmospheric Environment and Equipment Technology, School of Environmental Science and Engineering, Nanjing University of Information Science & Technology, Jiangsu Key Laboratory of Atmospheric Environment Monitoring and Pollution Control, Nanjing 210044, China
[c] College of Chemical and Environmental Engineering, Shandong University of Science and Technology, 266590 Qingdao, China

ARTICLE INFO

Keywords:
Core-Shell
Ni@SiO_2
Sintering-Free
Low carbon
CO_2 reforming with methane

ABSTRACT

Sintering-free and carbon-free Ni catalysts developments are hot topics for high temperature hydrocarbons catalytic reactions. Core-shell is a promising structure to limit sintering, but ineffective towards carbon deposition if big sized Ni nanoparticles are present. In this work, core-shell structured Ni@SiO_2 catalysts with small-sized Ni nanoparticles (about 5 nm) were synthesized by microemulsion method, which are featured by both sintering-free and low carbon deposits for high temperature CO_2 reforming with methane reaction. The advantages were originated from the silica shell overlay confined moving space of Ni nanoparticles and the small size of Ni nanoparticles guaranteed low carbon diffusion in Ni crystals. The work provides a simple approach to synthesize small-sized Ni nanoparticles in core-shell catalysts for stable performance of CO_2 reforming with methane reaction. It is supposed that this type of catalyst could also be applied in many other hydrocarbon catalytic reactions involving sintering and carbon problems.

1. Introduction

In last centuries, developments of scientific technologies and economies by consuming non-renewable fossil fuels had caused serious energy and environmental problems. Fossil fuels would be running out in near future if alternative energy resources were not maturely developed, and environmental disasters would be more often if solutions were not rightly taken. As an example, massive combustion of oil-based gasoline in vehicles and oxidation of organic chemicals in plants made abundant greenhouse gases emission into atmosphere. Greenhouse gases like CO_2, NO_x and CH_4 adsorb sunlight energy and make global warming, leading to glaciers melting, sea level rising, biological species extinction, and so on. Within the greenhouse gases, CO_2 contributes the highest impact to global warming. Nowadays, more and more researchers concentrated their effects on CO_2 reduction, in order to reduce CO_2 emission and utilize CO_2 to produce energy chemicals. This will help to solve both problems of global warming and energy shortage.

In literatures, techniques of heterogeneous catalytic, photocatalytic, electrochemical and biological CO_2 conversions have been extensively investigated for CO_2 utilization and emission reduction [1,2]. From points of engineering and industrialization, heterogeneous CO_2 catalytic conversion is the most promising approach than other methods because of the highest reaction rate of reactants and the fastest yield rate of products. Currently, CO_2 conversion to syngas, methane, methanol and other liquid fuels have been successfully realized by catalysis [3–6]. Among the products, syngas is an important raw chemical feedstock. Component of hydrogen or carbon monoxide can be separately purified for hydrogenation or carbonylation reactions, and mixture of hydrogen with carbon monoxide can applied to synthesize hydrocarbons through F-T process [7,8].

As one route for syngas production, CO_2 reforming with methane (CRM) is paid great attention because of the simultaneous reduction of green-house gases (CO_2 and methane). Up to date, kinds of catalysts have been explored for this reaction. Ni-based catalysts were the most extensively studied because of the stronger C—H bond breaking ability by Ni nanoparticles than other transitional metals nanoparticles [9–12]. However, Ni nanoparticles sintering and carbon deposition were happened during long-term run, resulting in poor performance stability [13]. The sintering enlarged metal size and decreased active sites, while the carbon deposits encapsulated catalysts surface and hindered contact of reactants [14]. Both of them caused a progressively performance decay with time on stream [15]. Therefore, it is a great challenge to develop Ni catalysts with features of constant Ni size and low carbon.

* Corresponding authors.
E-mail addresses: fagen.wang@gmail.com (F. Wang), swd1978@ujs.edu.cn (W. Shi).

https://doi.org/10.1016/j.apcatb.2018.04.069
Received 15 January 2018; Received in revised form 23 April 2018; Accepted 26 April 2018
Available online 27 April 2018
0926-3373/

It has been experimentally and thermodynamically reported that carbon deposits was closely correlated with Ni nanoparticle size for catalytic reactions [16–18]. On small-sized Ni nanoparticles, carbon deposition could be depressed because driving force of carbon diffusion in Ni crystals would be weakened [16]. Normally, Ni nanoparticle size should be less than 5 nm in order to minimize carbon deposits. [17–20] These works provide a very meaningful guidance that Ni catalysts would be performance stable if the size would be constant as small as possible. However, it is very difficult to maintain the small size because of particle migration or Ostwald Ripening effect [21]. Almost all small-sized Ni nanoparticles were aggregated for high temperature CRM reaction [9,22,23], especially on conventional Ni supported catalysts [23–25]. So maintaining small-size of Ni nanoparticles is one of key factors to obtain stable catalyst for CRM [12,26–29].

Recently, core-shell catalysts that have metal nanoparticles inside oxide overlay shell were viewed as potential candidates for size preservation [25,29–34]. This type of catalyst had been showed excellent advantages to resolve sintering problem for high temperature CRM reaction, such as Ni@SiO_2, Ni@silicalite-1 zeolite and Ni@Al_2O_3 [18,25,29,33–38]. Although stability was promoted due to the retarded or ignored metal sintering, carbon deposition was still observed in used catalysts. This should be associated with big size of Ni nanoparticles (more than 10 nm) and big diameter of silica spheres (more than 40 nm) in these works, showing relative abundant carbon diffusion in Ni crystals, and weak ability to gasify carbon precursors at metal-support boundaries.

In this work, we successfully prepared core-shell structured Ni@SiO_2 catalysts, in which small-sized Ni nanoparticles (around 5 nm) and small diameter of silica shell (around 30 nm) was obtained. The catalysts were applied for high temperature CRM reaction. Experiments results showed that the Ni@SiO_2 catalysts exhibited excellent Ni sintering-free feature due to SiO_2 shell confined moving spaces of the preserved small-sized Ni nanoparticles, which significantly reduced carbon deposits. Those contributed to unique stable performance for the high temperature CRM reaction.

2. Experimental

2.1. Chemicals

Chemicals of nickel nitrate, polyoxyethylene (n = 20) cety ether (PCE), cyclohexane, 50% hydrazine, tetraethyl orthosilicate, ammonia and isopropanol were bought from Sinopharm Co, Ltd. All the chemicals were directly used without pretreatment.

2.2. Catalysts preparation

Ni@SiO_2 catalysts with core-shell structure were prepared by water-in-oil microemulsion method, as described elsewhere[39]. Typically, polyoxyethylene (n = 20) cetyl ether and cyclohexane were homogeneously mixed by continuous magnetically stirring at room temperature. Aqueous nickel nitrate was introduced to form a transparent solution, followed by adding hydrazine to generate nitrate-hydrazine complex suspension. After reacted for 30 min at 323 K, tetraethyl orthosilicate and ammonia were put into the suspension, and were hydrolyzed for several hours. The obtained slurry was washed by isopropanol and hot water several times, dried at 333 K overnight and calcined at 1023 K for 2 h. For different hydrolysis times, catalysts were noted Ni@SiO_2-*t*, where t = 1 h, 2 h, 5 h and 10 h.

2.3. Catalysts characterization

Actual Ni contents on as-prepared catalysts were performed by inductively coupled plasma-atomic emission spectrometer (ICP-AES). Samples were firstly hydrothermal treated in HNO_3 to dissolve Ni species. Then supernatant was collected and was diluted to meet detection range of the spectrometer. Specific BET surface areas of the as-prepared catalysts were measured by a surface area analyzer (TriStar II 3020, Micromeritics) at 77 K. Before measurements, samples were heated to 573 K for 3 h under vacuum to remove contaminates and water.

X-ray powder diffraction (XRD) patterns of the as-prepared catalysts were conducted by X-ray diffractor (XRD-6100x, Shimadzu) using Cu-K_α (λ = 1.5406 Å) radiation. The measurement was conditioned at 40 kV and 30 mA, scanning speed 7°/min from 10° to 70°. Crystalline size of Ni species was calculated according to the Scherrer Equation [40].

Transmission electron microscopy (TEM) images of samples were taken by a transmission electron microscope JEOL 2010 operated at 200 kV. Specimens were prepared by dispersing samples in ethanol and droplets of the suspension were deposited on a thin copper grid. After ethanol was vaporized, the thin copper grid was inserted into sample chamber of the transmission electron microscope.

H_2 temperature-programmed reduction (H_2-TPR) of the as-prepared catalysts were performed by an apparatus equipped with a thermal conductivity. Prior to the experiments, samples were pretreated at 573 K for 2 h under flowing N_2 (30 mL/min) to remove impurities. After cooling to 298 K, a mixture of 10%H_2/N_2 (30 mL/min) was introduced to get a stable baseline. The catalysts were then heated to 1023 K at a rate of 5 K/min.

Temperature-programmed oxidation (TPO) of used catalysts were performed in a mass spectrometer (PrismaPlus, Pfeiffer). The used samples were thermally treated by N_2 (30 mL/min) at 573 K to clear contaminants, and then were programmable heated to 1073 K by 5% O_2/N_2 (30 mL/min). Signal of CO_2 (m/e = 44) was monitored by the mass spectrometer (PrismaPlus).

Thermogravimetric (TG) analysis of the used samples was carried on by an Integrated thermal analyzer (STA 449 C) from 293 K to 1073 K at a rate of 10 K/min under air atmosphere.

2.4. Catalytic activity and stability tests

Catalytic activity measurements of CRM over the Ni@SiO_2 catalysts were performed in a fixed-bed reactor (internal diameter 6 mm, length 300 mm). 100 mg catalyst was loaded in the reactor and was in-situ reduced by 30%H_2/N_2 (30 mL/min) at 1023 K. The reactor was then cooled to 873 K by purging N_2 (30 mL/min). A mixture of equimolar CH_4/CO_2 (30 mL/min) was passed through the catalyst and was mixed with internal standard gas of N_2 (20 mL/min). Catalytic performance was evaluated from 873 K to 1023 K. Products of CO, H_2, CH_4 and CO_2 in outlet were separated by a packed column (TDX-01), and then analyzed by an on-line gas chromatography (Fuli 7890II) equipped with a TCD. Conversions of CH_4 and CO_2, space-time yields of products (H_2 and CO), as well as molar ratio of H_2/CO were determined from corresponding flow rates in the inlet and outlet [39].

$$\text{Methane conversion: } X_{CH_4} = \frac{F_{CH_4,inlet} - F_{CH_4,outlet}}{F_{CH_4,inlet}} \times 100\% \quad (1)$$

$$\text{Carbon dioxide conversion: } X_{CO_2} = \frac{F_{CO_2,inlet} - F_{CO_2,outlet}}{F_{CO_2,inlet}} \times 100\% \quad (2)$$

$$\text{Space-time yield of } H_2\text{: } STY_{H_2} = \frac{F_{H_2,outlet}}{m_{cat}} \quad (3)$$

$$\text{Space-time yield of CO: Space-time yield of CO: } STY_{CO} = \frac{F_{CO,outlet}}{m_{cat}} \quad (4)$$

$$\text{The molar ratio of } H_2 \text{ to CO: } \frac{n_{H_2}}{n_{CO}} = \frac{F_{H_2,outlet}}{F_{CO,outlet}} \quad (5)$$

where *Fi* represents the flow rate of *i* species (mol/min).

Table 1
Texture properties of the as-prepared and the used Ni@SiO_2 catalysts.

Catalysts	Ni loading[a] (%)	Ni size[b] (nm)	SiO_2 shell thickness[b] (nm)	SiO_2 nanospheres diameter[b](nm)	BET surface area[c] (m^2/g)	Average pore size[c] (nm)	Average pore volume[c] (cm^3/g)
Ni@SiO_2-1 h	3.6	3.4	11.3	31.1	222	16.4	1.04
Ni@SiO_2-2 h	2.7	4.3	10.2	29.5	153	18.9	0.82
Ni@SiO_2-5 h	2.7	4.1	12.3	30.7	147	15.4	0.65
Ni@SiO_2-10 h	2.6	4.7	10.4	30.2	143	17.7	0.74
Used Ni@SiO_2-1 h	-[d]	4.8	10.1	30.5	–	–	–
Used Ni@SiO_2-2 h	–	5.6	10.7	29.3	–	–	–
Used Ni@SiO_2-5 h	–	5.5	11.9	32.7	–	–	–
Used Ni@SiO_2-10 h	–	6.3	10.2	29.7	–	–	–

Notes:
[a] ICP results.
[b] average Ni size / silica shell thickness / silica nanospheres diameters were obtained from TEM images by counting more than 500 nanoparticles in reduced or used samples.
[c] values are measured from nitrogen adsorption-desorption curves.
[d] Not measured.

2.5. Turnover frequency (TOF) of methane and activation energy measurements.

Kinetic experiments were conducted in the same fixed-bed reactor mentioned above. 5 mg Ni@SiO_2-1 h catalyst powder (80–100 mesh) diluted with 250 mg SiC was loaded, and the height of catalyst bed was about 12 mm. Activation energy of CH_4 was calculated by controlling CH_4 conversion below 15% within temperature range of 823–973 K at 15 ml/min flow rate of CH_4.

3. Results and discussions

3.1. Texture properties of the as-prepared Ni@SiO_2 catalysts

Table 1 shows ICP results of the as-prepared Ni@SiO_2 catalysts synthesized at different hydrolysis times. The actual contents of Ni were 3.6 wt%, 2.7 wt%, 2.7 wt% and 2.6 wt% on Ni@SiO_2-1 h, Ni@SiO_2-2 h, Ni@SiO_2-5 h and Ni@SiO_2-10 h catalysts, respectively. Nitrogen adsorption-desorption isotherms of the Ni@SiO_2-*t* (*t* = 1 h, 2 h, 5 h and 10 h) catalysts (Fig. 1) exhibit Type-IV adsorption isotherms, suggesting the presence of mesoporous in the samples. The inserted pore distribution plots reaffirmed mesoporous formation, within which two domain pore sizes were measured. One sharp peak is centered at around 10 nm, and another broad peak is ranged 15–60 nm. The average pore size of the Ni@SiO_2-1 h, Ni@SiO_2-2 h, Ni@SiO_2-5 h and Ni@SiO_2-10 h catalysts were 16.4 nm, 18.9 nm, 15.4 nm and 17.7 nm, respectively, and the average pore volumes were corresponding to 1.04 cm^3/g, 0.82 cm^3/g, 0.65 cm^3/g and 0.74 cm^3/g. Multipoint analysis of the isotherms reveals that BET surface areas were 222 m^2/g, 153 m^2/g, 147 m^2/g and 143 m^2/g for the catalysts of Ni@SiO_2-1 h, Ni@SiO_2-2 h, Ni@SiO_2-5 h and Ni@SiO_2-10 h, respectively.

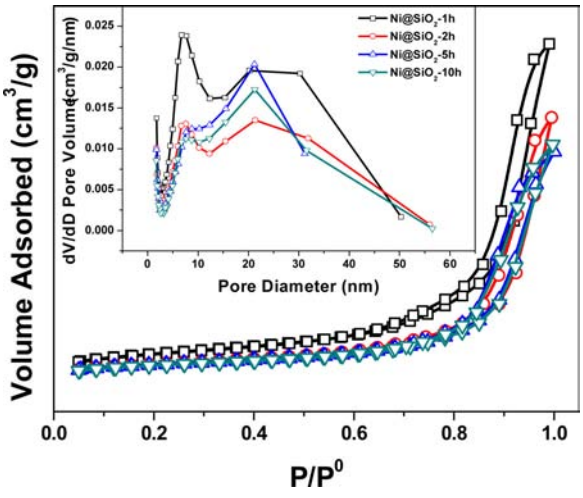

Fig. 1. N_2 adsorption-desorption isotherm plots and pore distributions of the Ni@SiO_2 catalysts.

XRD patterns (Fig. 2A) of the as-prepared Ni@SiO_2-*t* (*t* = 1 h, 2 h, 5 h and 10 h) catalysts display a widen diffraction peak at around 2theta = 23.5°, suggesting the presence of amorphous silica. Broad diffraction peaks of NiO(111) and NiO(200) were detected on the Ni@SiO_2-1 h catalyst, while were not obviously measured on the other catalysts. The broadened NiO diffraction peaks suggested that small sized NiO nanoparticles were formed in the Ni@SiO_2-1 h, and the undetectable NiO signals indicated that NiO contents were much low or NiO dispersions were high in the other catalysts. After hydrogen reduction treatment, widen diffraction peaks of amorphous silica were still observed, while diffraction peaks of metallic Ni were not clearly recorded (Fig. 2B). This indicates that Ni nanoparticles were highly dispersed in the reduced catalysts.

TEM images of reduced Ni@SiO_2 catalysts (Fig. 3) clearly show nanoparticles of Ni and shell overlay of silica nanospheres, confirming the construction of core-shell structured catalysts. Some relative big sized (5–8 nm) Ni nanoparticles were positioned in cavity of silica nanospheres, and some small sized (2–5 nm) Ni nanoparticles were embedded in shell of silica nanospheres. The images evidenced that all the Ni nanoparticles were successfully confined or encapsulated by the silica overlay. The average sizes of Ni nanoparticles were around 3.4–4.7 nm and the mean diameters of silica nanospheres were 29.5–31.1 nm for the reduced Ni@SiO_2-*t* (*t* = 1 h, 2 h, 5 h and 10 h) catalysts. Besides, cavity was formed inside the silica nanospheres, average thickness of the cavity was 10.2–12.3 nm. Considering the catalysts were all hydrogen-reduction treated at high temperature of 1023 K, the small-sized Ni nanoparticles formation should be attributed from encapsulation and protection of silica nanospheres that confined moving spaces and thus limited sintering. The TEM results demonstrated that the structure, as well as dimensions of Ni nanoparticles and silica nanospheres, were not significantly influenced by longing hydrolysis time during catalysts preparation process.

H_2-TPR profiles of the as-prepared Ni@SiO_2 catalysts (Fig. 4) display two reduction domains. The first broad reduction peak between 600 K and 833 K should be assigned to NiO species that have weak interaction with silica shell. The second broad peak from 850 K to 1000 K could be attributable to NiO species that have strong interaction with silica shell. Generally, reduction ability of small sized NiO nanoparticles should be higher than that of big sized NiO nanoparticles [41]. Due to the close silica shell thicknesses and average pore sizes in the

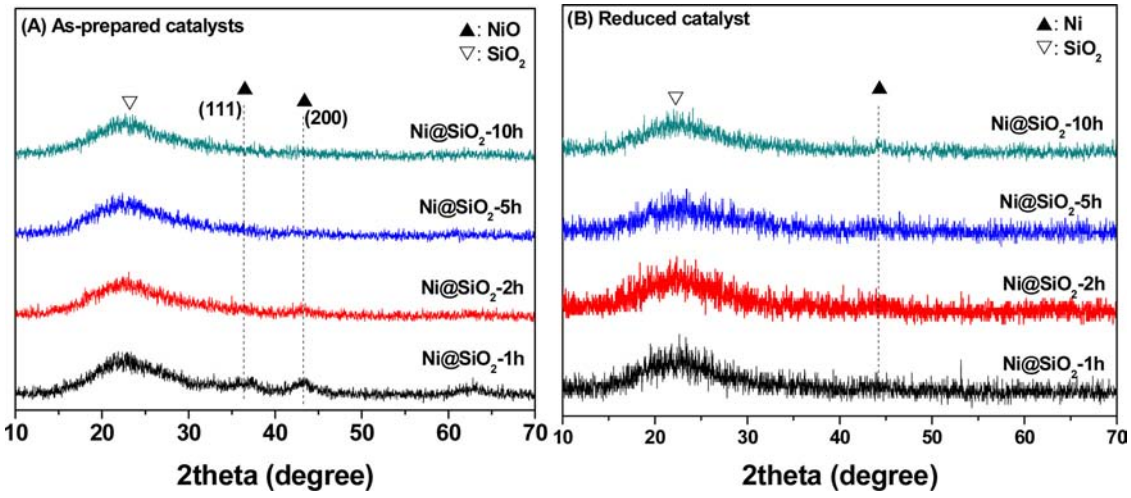

Fig. 2. X-ray diffraction patterns of (A) the as-prepared and (B) the reduced Ni@SiO_2 catalysts.

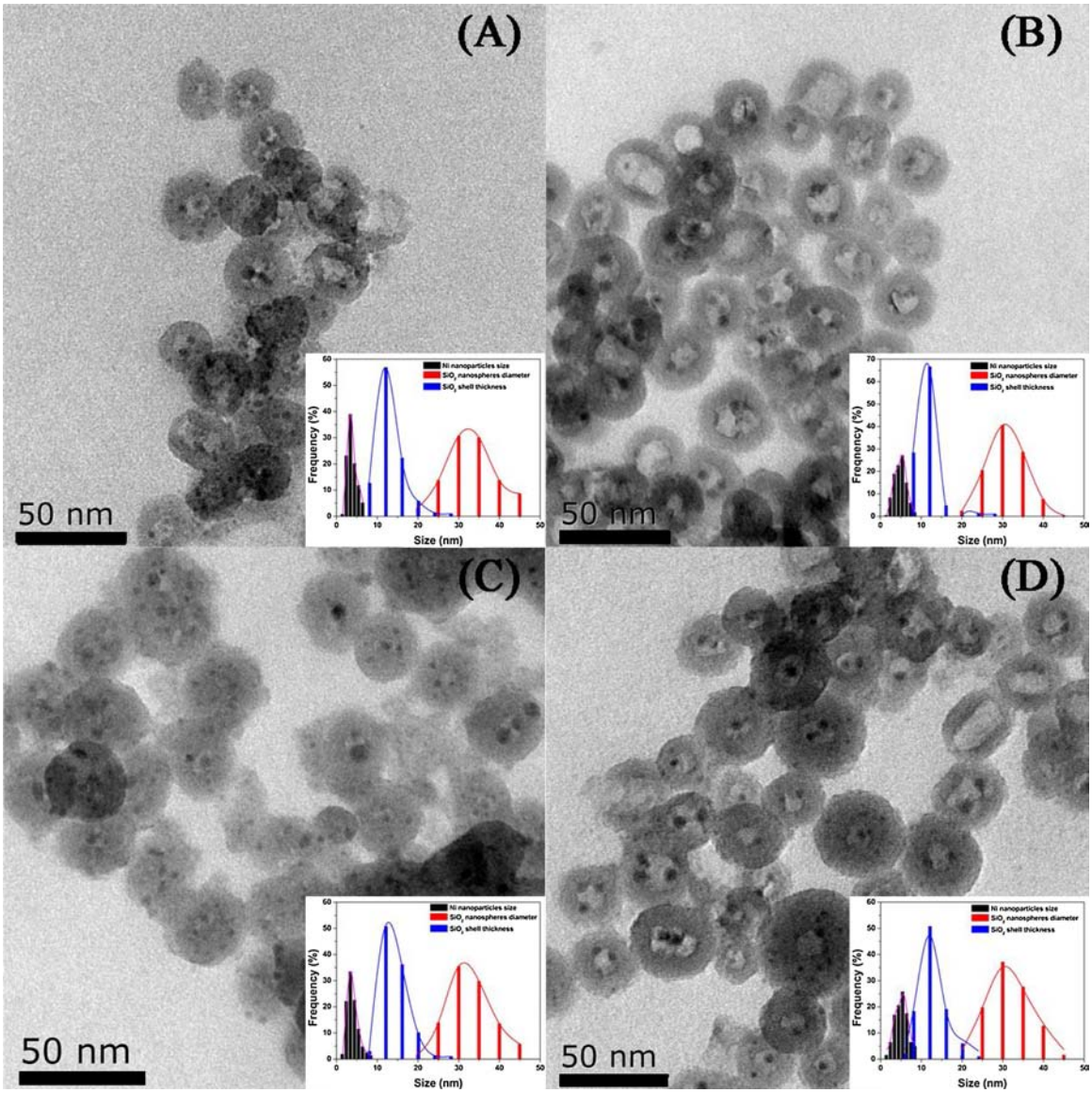

Fig. 3. TEM images of the reduced Ni@SiO_2 catalysts. (A) Ni@SiO_2-1 h, (B) Ni@SiO_2-2 h, (C) Ni@SiO_2-5 h and (D) Ni@SiO_2-10 h.

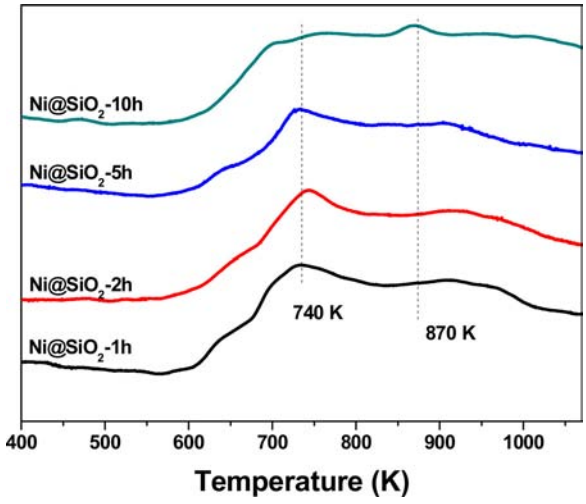

Fig. 4. H_2-TPR profiles of the as-prepared Ni@SiO_2 catalysts.

Ni@SiO_2-*t* (*t* = 1 h, 2 h, 5 h and 10 h) catalysts, the former reduction might be from small NiO species that embedded in the silica overlay, and the latter reduction should be related to big NiO species that located in the cavity of silica shell [34]. Additionally reduction of Ni silicate species was observed above 973 K by S. Kawi et al. in their Ni@SiO_2 catalysts [33,34], while was not obviously measured in the current catalysts, suggesting the non-existence of Ni silicate species in the Ni@SiO_2 catalysts.

3.2. Catalytic performance and stability tests of high temperature CO_2 reforming with methane over the Ni@SiO_2 catalysts

3.2.1. Internal diffusion limitations analysis

The confinement of Ni nanoparticles in silica overlay might result in internal diffusion limitation if the silica overlay contains much porous (microporous or mesoporous) and the silica nanospheres is too thick. Those would slow diffuse rate of reactants from silica external to silica internal, as well as to Ni nanoparticles. To confirm this, Weisz-Prater criteria (C_{WP}) and Thiele Modulus Φ_n were applied to evaluate the internal diffusion, and Mears criterion (C_M) was used for combined interphase and intra-particle heat and mass transport for CH_4 at 823 K [37,42].

$$\text{Weisz-Prater criterion: } C_{WP} = \frac{-r_{A(obs)}\rho_c R^2}{D_e C_{As}} \tag{6}$$

$$\text{Thiele Modulus criterion: } \Phi_n = R\sqrt{\frac{-r_A \cdot \rho_c}{D_e \cdot C_{As}}} \tag{7}$$

$$\text{Mears criterion: } C_M = \frac{-r_A R^2}{C_{Ab} D_e} \tag{8}$$

where $-r_{A(obs)}$ is measured reaction rate, ρ_c is density of solid catalyst, R is radius of the catalyst particle, D_e is effective diffusivity, C_{As} is reactant concentration external to the pellet, C_{Ab} is bulk gas concentration of A.

Take the catalyst of Ni@SiO_2-1 h as an example, results show that C_{WP} = 1.003, Φ_n = 1.002 and $C_M = 4.56 \times 10^{-4}$. Both the values of C_{WP} and Φ_n are close to the criteria values of 1, and C_M is far less than the criterion value of 3. The criteria suggested that the interphase and intra-particle heat and mass transport could be ignored for CH_4, but internal diffusion was slightly occurred during the reaction. However, this internal diffusion was not so serious, which should not affect the measurements of turnover frequency and apparent activation energy below.

Besides, preliminary experiments were conducted on by loading different mass of catalysts and by varying catalysts particle sizes at the same GHSV, in order to evaluate criteria of interphase mass transport resistance and intra-particle mass transfer resistance for CH_4. The internal mass transport resistance criterion was done by keeping constants of contact time, molar ratio of CH_4/CO_2, particle size of catalyst and reaction temperature, changing reactants flow rate and mass of catalyst to measure CH_4 conversions. The result (Supplementary Information, Fig. S1(A)) showed that CH_4 conversions were almost constant at high flow rate, demonstrating a very marginal internal mass transport resistance, which is good agreed with the above Weisz-Prater and Thiele Modulus criteria. The occurrence of inter-particle transport resistance was checked by preserving CH_4/CO_2 molar ratio and contact time, and varying the catalyst particle size from 100 mesh to 40 mesh. The result (Supplementary Information, Fig. S1(B)) revealed that CH_4 conversions were also maintained at all ranges of particle size, suggesting that inter-particle transport resistance was not severely happened, which is coincided with the previous Mears criterion.

3.2.2. Turnover frequency (TOF) and apparent activation energy E_a

It has been considered that dissociative adsorption of CH_4 was rate-determining step for CRM reaction, turnover frequency (TOF) value of CH_4 could be applied for activity comparison [10]. In order to further demonstrate the excellent performance of the Ni@SiO_2 catalysts for CRM reaction, TOF was measured by controlling methane conversion below 15% at 823 K. As shown in Table 2, TOF of methane was measured 361 h^{-1} over the Ni@SiO_2-1 h catalyst, followed by Ni@SiO_2-2 h, Ni@SiO_2-5 h and Ni@SiO_2-10 h catalysts. The TOFs in the Ni@SiO_2 catalysts were close to the ones in Ni/SBA-15 catalysts, which had been demonstrated as an excellent carbon- and sintering-resistance in CRM reaction [43]. Therefore, it is reasonable that the Ni@SiO_2 catalysts might exhibit advantages of carbon- and sintering-resistance towards CRM because Ni nanoparticles were confined in SiO_2 nanospheres, which is the same as Ni nanoparticles confined in SBA-15 mesoporous. Other researchers reported very large TOFs of methane over various Ni@SiO_2 catalysts at 1073 K [25,33,34,36], which was much higher than the current 823 K.

Apparent activation energy (E_a) of methane was measured to be 51.6 kJ/mol over the Ni@SiO_2-1 h catalyst (Supplementary Information, Fig. S2), which is agreed with pioneers' results from 40.8 kJ/mol to 105 kJ/mol (Table 2). The E_a was close to Ni/SiO_2 catalyst (E_a = 62.3 kJ/mol) and La-promoted Ni/SBA-15 (40.8 kJ/ml) [44,45], although much less than Ni/SiO_2@SiO_2 catalyst (E_a = 93.5 kJ/mol) [18]. The differences should be associated with different textures or structures of catalysts that had different abilities in methane activation and diffusion, such as size of Ni nanoparticles, average pore size of SiO_2 overlay or diameter of SiO_2 nanospheres. The E_a of methane over the Ni@SiO_2-1 h catalyst belongs to low range of activation energy values reported in literatures for confined Ni catalysts (including

Table 2
Comparisons of Ea and TOFs of CRM over the Ni@SiO_2 catalysts with References.

Catalysts	CH_4		D_{Ni} (%)	Refs.
	E_a (kJ/mol)	TOF (h^{-1})		
Ni@SiO_2-1 h (823 K)	51.6	361	29.4	This work
Ni@SiO_2-2 h (823 K)	Not available (N. A.)	265	23.2	This work
Ni@SiO_2-5 h (823 K)	N. A.	229	24.3	This work
Ni@SiO_2-10 h (823 K)	N. A.	213	21.3	This work
Ni/SBA-15-EG (823 K)	N. A.	228	14.1	[43]
Ni/SBA-15-H_2O (823 K)	N. A.	208	14.1	[43]
Ni/SBA-15-GC (823 K)	N. A.	225	14.1	[43]
La-Ni/SBA-15	40.8	N. A.	33.3	[45]
Ni/SiO_2@SiO_2	93.5	N. A.	N. A.	[18]
Ni/SiO_2	62.3	N. A.	N. A.	[44]
Ni/MgO	105	N. A.	14.8	[55]
Ni/ZrO_2-f-u (1023 K)	N. A.	254	12.1	[56]
Ni/La_2O_3 (1023 K)	62.7	N. A.	N. A.	[57]

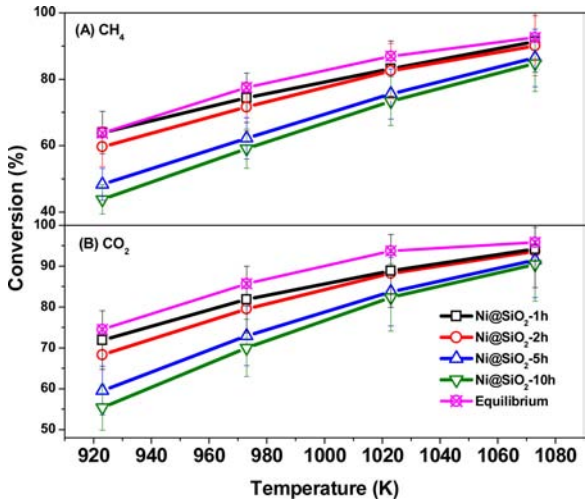

Fig. 5. Conversions of CH_4 and CO_2 over the Ni@SiO_2 catalysts and thermodynamic conversions of CH_4 and CO_2 as a function of temperature.
Reaction conditions: mass of catalyst: 100 mg, Flow rate = 30 mL/min, molar ratio: CH_4/CO_2 = 1, P = 0.1 MPa.

confined in ordered mesoporous material [43] and encapsulated in silica [18]), indicating that methane could be effectively activated by Ni nanoparticles, associating with their smaller size that exposed more surface atoms hosting and transforming methane molecules.

3.2.3. Catalytic performance of CO_2 reforming reaction over the Ni@SiO_2 catalysts

From the point of view in industrial application, high pressure was always required for heterogeneous gaseous reactions, such as 2 MPa or above. While for the reaction of CRM, experimental and thermodynamic investigations revealed that the higher pressure exhibited negative effects towards the conversions of methane and carbon dioxide [46–48]. This means that the conversions at high pressure were lower than those at low pressure (Supplementary Information, Fig. S3). Therefore, in order to have relative high conversions of CH_4 and CO_2 to maximize the greenhouse gases' utilization, low pressure (1 atm or 0.1 MPa) was chosen for performance measurements and stability tests in the current study.

Catalytic performance results (Fig. 5) show that conversions of methane and carbon dioxide were highly dependent on reaction temperature. The higher reaction temperature promoted the higher conversions of methane and carbon dioxide, which was coincided with the endothermic characteristics of CRM reaction ($CO_2(g) + CH_4(g) \rightarrow 2CO(g) + 2H_2(g)$, $^{\triangle}H_{298} = +247$ kJ/mol) [49]. At 923 K, conversions of methane and carbon dioxide were 43% and 55%, respectively, over the Ni@SiO_2-10 h catalyst, while the corresponding conversions were 63% and 71% over the Ni@SiO_2-1 h catalyst. At 1073 K, 85% methane and 90% carbon dioxide were converted over the Ni@SiO_2-10 h catalyst, and 91% methane and 94% carbon dioxide were transformed over the Ni@SiO_2-1 h catalyst. The measurements clearly suggested the influence of hydrolysis time on the catalytic performance of CRM reaction. The longer hydrolysis time of the Ni@SiO_2 would resulted in the relative lower conversions of methane and carbon dioxide, which should be originated from the differences of textures.

Thermodynamic conversions depending on temperature were conducted by software 6.0 and were compared with the ones measured from experiments above, the result showed that the thermodynamic values were very close to experimental catalytic performance of CO_2 reforming reaction over the current Ni@SiO_2 catalysts, suggesting the very efficient catalytic activity of the Ni@SiO_2 catalysts, especially for Ni@SiO_2-1 h and Ni@SiO_2-2 h catalysts.

It is acknowledged that the higher metal loading and the smaller metal nanoparticles size would contribute to expose more metal active sites, and the higher BET surface area would help to adsorb more reactants. Those should beneficial for the higher catalytic reaction performances [19,50]. From Table 1, the above texture properties of Ni@SiO_2 catalysts show some connections with hydrolysis time. The Ni@SiO_2-1 h catalyst possessed the highest Ni loading, the smallest average Ni nanoparticle size and the highest BET surface area, which should be contributed to the highest activity for conversions of methane and carbon dioxide. The texture properties were slightly decreased when the hydrolysis time was longer, which could be accounted for the slightly reduced performance over other Ni@SiO_2 catalysts.

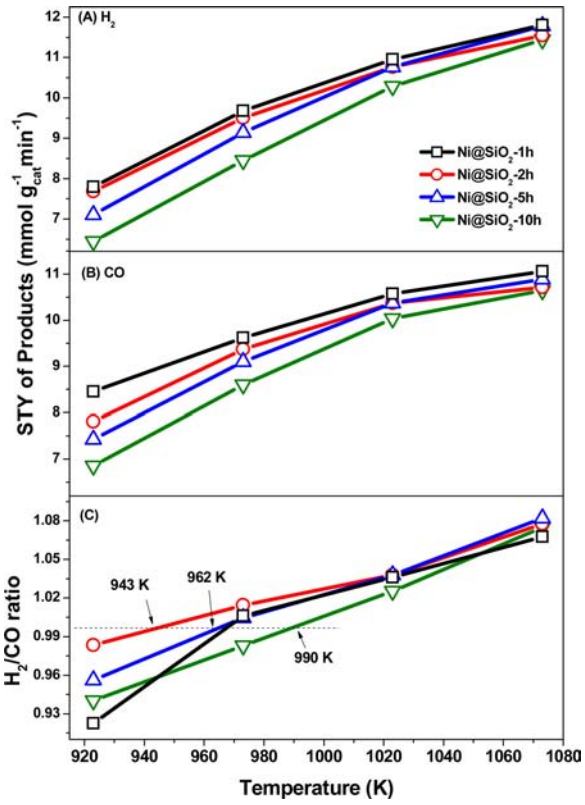

Fig. 6. (A) H_2 yield rate, (B) CO yield rate and (C) H_2/CO molar ratio of methane dry reforming reaction over the Ni@SiO_2 catalysts at different temperatures.
Reactions conditions: mass of catalyst: 100 mg, Flow rate = 30 mL/min, molar ratio: CH_4/CO_2 = 1, P = 0.1 MPa.

Space-time yields of products (H_2 and CO) (Fig. 6A and B) at different temperatures over the Ni@SiO_2 catalysts follow the similar trend of conversions of methane and carbon dioxide, suggesting agreements of reactants conversions with products yield rates. Specifically, yields of H_2 and CO were 6.44 $mmol g_{cat}^{-1} min^{-1}$ and 6.85 $mmol g_{cat}^{-1} min^{-1}$, respectively, at temperature of 923 K, and were accordingly increased to 11.44 $mmol g_{cat}^{-1} min^{-1}$ and 10.64 $mmol g_{cat}^{-1} min^{-1}$ at temperature of 1073 K over the Ni@SiO_2-10 h catalyst. In the same way, H_2 and CO yields were 7.80 $mmol g_{cat}^{-1} min^{-1}$ and 8.45 $mmol g_{cat}^{-1} min^{-1}$, respectively, at 923 K, and were correspondingly enhanced to 11.80 $mmol g_{cat}^{-1} min^{-1}$ and 11.06 $mmol g_{cat}^{-1} min^{-1}$ with the temperature was increased to 1073 K over the Ni@SiO_2-1 h catalyst. The products yield rates were also dependent on the hydrolysis time of Ni@SiO_2 catalysts, higher yields of products were obtained over the Ni@SiO_2 catalyst synthesized at the shorter hydrolysis time.

Molar ratio of H_2/CO (Fig. 6C) was progressively increased with reaction temperature, varying from 0.92 to 0.98 at 923 K to 1.05–1.08 at 1073 K. Normally, molar ratio of H_2/CO should be 1 ($CH_4 + CO_2 \rightarrow 2CO + 2H_2$) when equal-conversions of methane and carbon dioxide are achieved. However, because of the reactants conversions were

different (Fig. 5), molar ratio of H_2/CO was not equal to 1, suggesting other reactions should be involved during the course of CRM. If molar ratio of H_2/CO was less than 1, reverse water gas shift reaction ($CO_2 + H_2 \rightarrow CO + H_2O$) should be occurred, while if the molar ratio was more than 1, reaction of methane decomposition ($CH_4 \rightarrow C + H_2$) or steam reforming of methane ($CH_4 + H_2O \rightarrow CO + 3H_2$) might be involved. In Fig. 6C, temperatures might be 965 K, 943 K, 962 K and 990 K when molar ratio of H_2/CO was 1 for the Ni@SiO_2-1 h, Ni@SiO_2-2 h, Ni@SiO_2-5 h and Ni@SiO_2-10 h catalysts, respectively. Below the temperature, reverse water gas shift reaction should be taken place over the corresponding catalyst.

3.2.4. Stability tests of CO_2 reforming reaction over the Ni@SiO_2 catalysts

As one of the main causes that deactivating Ni catalysts [46–48], carbon deposition should be minimized as much as possible to maintain stable performance of CO_2 reforming reaction. Due to carbon deposits were rather prohibitive at industrial level because high pressure benefits to deposit carbon species (Supplementary Information, Fig. S4) [51,52], stability tests of CO_2 reforming reaction over the Ni@SiO_2 catalysts were conducted at low pressure of 0.1 MPa, which was the same as above.

Products yield rates as function of time on stream were tested to evaluate performance stability of CRM reaction over the Ni@SiO_2 catalysts. Results shown in Fig. 7 illustrate that all the catalysts could exhibit stable production rates within 50 h on stream. H_2 and CO yield rates were maintained at 10.7–10.5 $mmol g_{cat}^{-1} min^{-1}$ and 10.3–10.0 $mmol g_{cat}^{-1} min^{-1}$, respectively, and molar ratio of H_2/CO was preserved at about 1.04 over the Ni@SiO_2-1 h catalyst. Production rates of H_2 and CO were constant at 10.4–10.1 $mmol g_{cat}^{-1} min^{-1}$ and 10.2–10.0 $mmol g_{cat}^{-1} min^{-1}$, and molar ratio of H_2/CO was kept at around 1.01 during stability tests over the catalyst of Ni@SiO_2-2 h and Ni@SiO_2-5 h. Slightly lower products rates were observed for the Ni@SiO_2-10 h catalyst, over which H_2 yield rate was 8.5–8.3 $mmol g_{cat}^{-1} min^{-1}$, CO yield rate was 8.6-8.4 $mmol g_{cat}^{-1} min^{-1}$, and molar ratio of H_2/CO was about 0.99. Carbon balance (Fig. 7D) during the stability test of CRM reaction was in range of 95%–102%, suggesting that CO could be fully produced from CH_4 and CO_2, and almost no carbon deposition was left on the catalyst surface. The ignorable carbon deposition could be verified by TG results of used catalysts that discussed below.

Based on pioneers' works, Ni nanoparticles sintering and carbon deposition were two main causes that resulted in catalyst deactivation [13,14,20,23,53]. Those would enlarge Ni nanoparticle size (sintering) and encapsulate Ni nanoparticles (carbon deposits). In the current case, catalytic performance deactivation was not obviously measured over the Ni@SiO_2-t (t = 1 h, 2 h, 5 h and 10 h) catalysts. Both yields of H_2 and CO, as well as molar ratio of H_2/CO, could be maintained within the testing hours, suggesting an unique stability for high temperature CRM reaction. This should be related with the intrinsic structure of the core-shell Ni@SiO_2 catalysts that could effectively avoid Ni sintering by confining moving space, and could significantly reduce carbon deposition by maintaining the small size of Ni nanoparticles, which will be demonstrated in the following characterizations of used catalysts.

3.3. Characterizations of used Ni@SiO_2 catalysts after stability tests

After the stability tests at conditions of GHSV = 18,000 mL/(gh) and 1023 K for 50 h, the used Ni@SiO_2 catalysts were applied for characterizations of XRD, TEM, TPO and TG, in order to further illustrate the excellent features of Ni-sintering free and low carbon deposits in the small-sized Ni@SiO_2 catalysts.

XRD records of the used Ni@SiO_2 catalysts (Fig. 8) display two broad peaks at 23.5° and 44.3°. The former is assign to amorphous silica, and the latter is attributed to Ni(111). In comparison with the XRD patterns of the reduced Ni@SiO_2 catalysts (Fig. 2B), one major difference is from the diffraction intensities of Ni nanoparticles. The absent

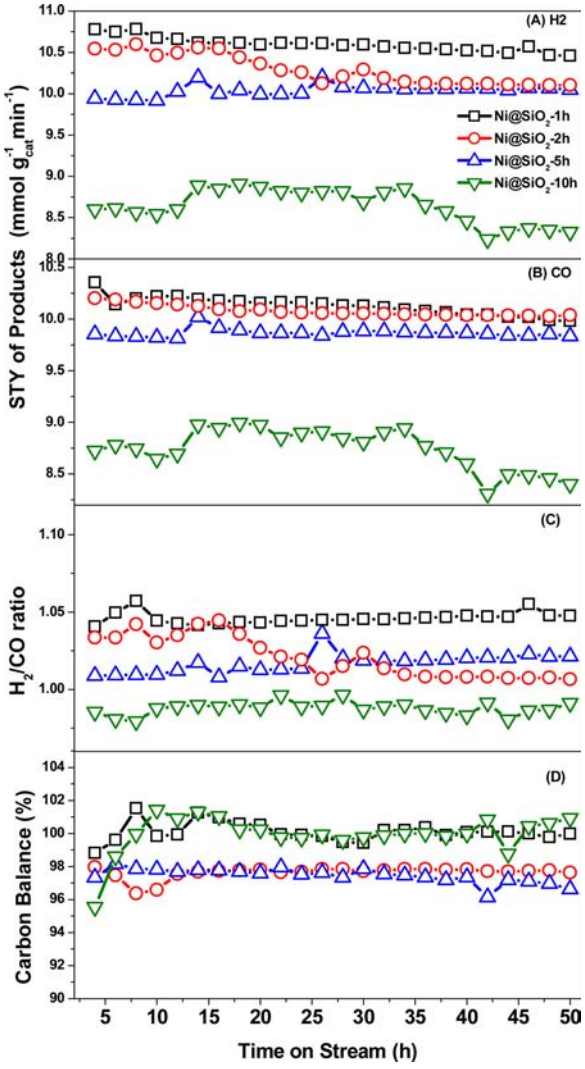

Fig. 7. Stability tests of (A) H_2 yield rate, (B) CO yield rate, (C) H_2/CO molar ratio and (D) Carbon balance of CO_2 reforming with methane reaction over the Ni@SiO_2 catalysts at 1023 K.
Reaction conditions: mass of catalyst: 100 mg, Flow rate = 30 mL/min, molar ratio: CH_4/CO_2 = 1, P = 0.1 MPa.

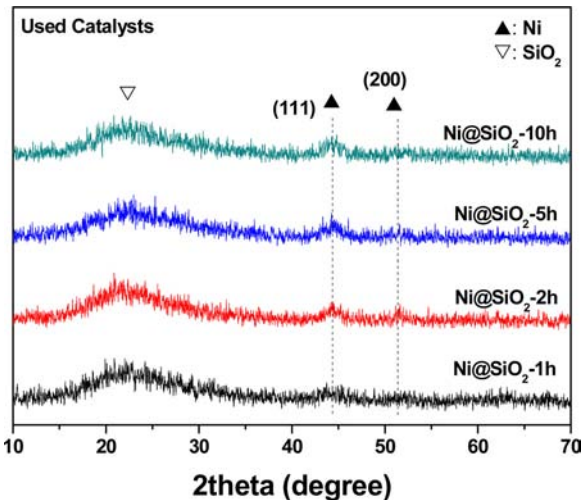

Fig. 8. X-ray diffraction patterns of the used Ni@SiO_2 catalysts.

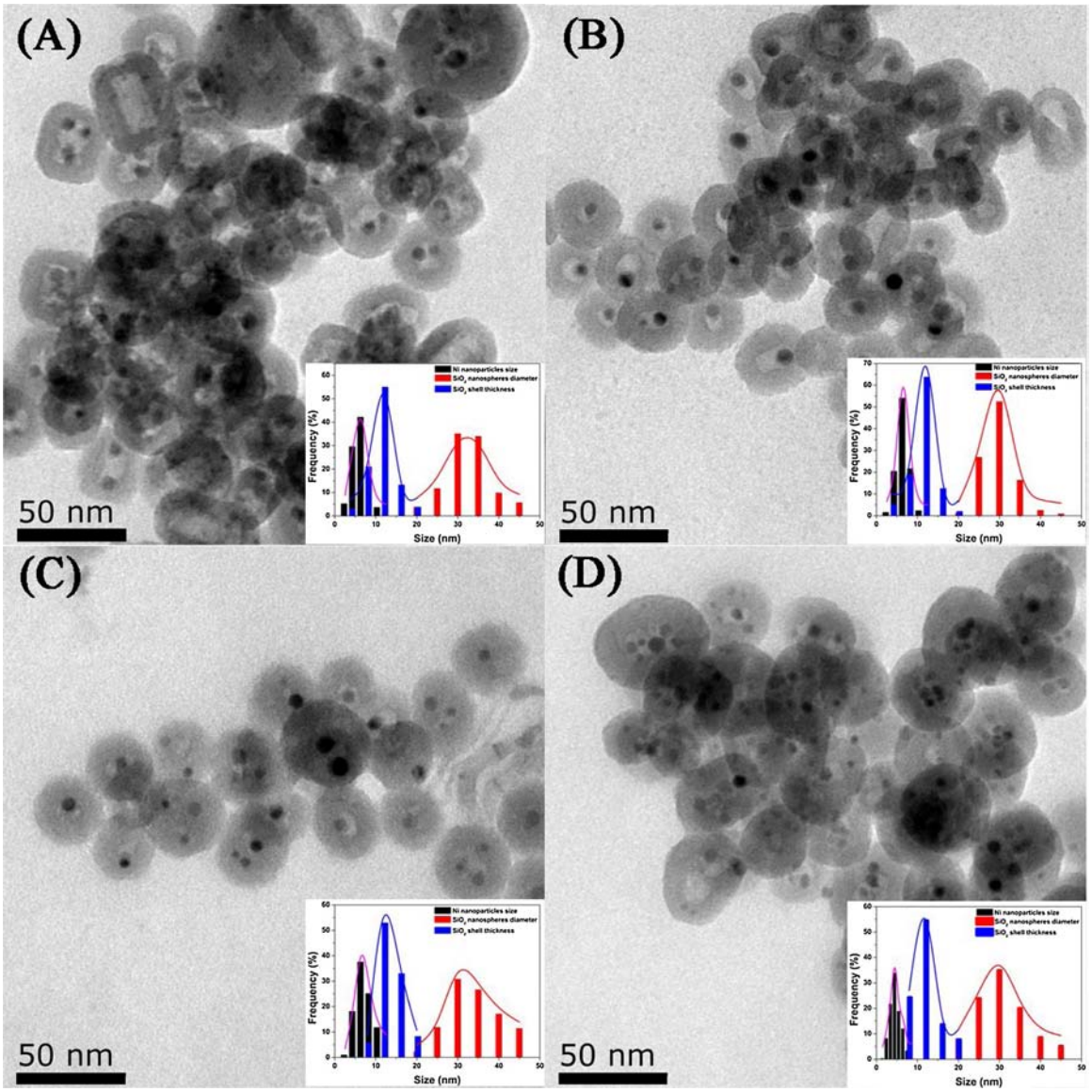

Fig. 9. TEM images of the used Ni@SiO_2 catalysts. (A) Ni@SiO_2-1 h, (B) Ni@SiO_2-2 h, (C) Ni@SiO_2-5 h and (D) Ni@SiO_2-10 h.

signals of Ni(111) in Fig. 2B suggested small size of Ni nanoparticles in the reduced Ni@SiO_2 catalysts, while the present signals of Ni(111) in Fig. 8 indicated relative big size of Ni nanoparticles in the used Ni@SiO_2 catalysts. This seems that slightly Ni nanoparticle sintering was occurred after stability test. However, it should be noted that the widen diffraction peaks of Ni(111) implied big line broadening width at half the maximum intensity (FWHM), which should also give small size of Ni nanoparticles. Due to weak peaks intensities, Ni nanoparticles sizes could not accurately calculated from Scherrer Equation, but will be analyzed by TEM.

TEM images of the used Ni@SiO_2 catalysts (Fig. 9) demonstrate that all the used samples maintained the core-shell structure, composing of Ni nanoparticles in core center and silica overlay in shell. The average sizes of Ni nanoparticles were about 5.3 nm, 5.6 nm, 5.5 nm and 6.3 nm in the used catalysts of Ni@SiO_2-1 h, Ni@SiO_2-2 h, Ni@SiO_2-5 h and Ni@SiO_2-10 h, respectively, which were very close to those in the reduced samples (Table 1). The marginally size variation suggested that Ni nanoparticles sintering was not taken place. This excellent sintering-free feature should be originated from confinement effect of silica shell, which confines moving spaces of Ni nanoparticles and thus avoids aggregation. The average silica diameters and silica shell thickness were 29.3–32.7 nm and 10.1–11.9 nm, respectively, which were also close to the corresponding values in the reduced catalysts (Table 1). Those almost unchanged dimensions of silica nanospheres, as well as the maintained size of Ni nanoparticles, confirmed a retained structure after suffering high temperature reaction for long hours. Those should be considered as one contribution for stable catalytic performance of CO_2 reforming reaction shown in Fig. 7.

Another contribution for the stable performance should be associated with hardly carbon deposition in the used Ni@SiO_2 catalysts under the current low pressure condition, which thermodynamically favors lower carbon deposition when compared with that in high pressure (Supplementary Information, Fig. S4). As displayed in the TEM images, there were no severe formation of carbon deposits observed. The few carbon deposition might be associated with the relative thicker silica shell and the small Ni nanoparticle size. It has been suggested that negligible carbon could be produced when silica shell thickness was greater than 8.6 nm [33], and driving force of carbon diffusion in Ni crystals could be weakened if size of Ni nanoparticles was less than 5 nm [16]. Both of them would attributed to formation of soft carbon (C_α, adsorbed atomic carbon or amorphous carbon), which can be partially gasified by CO_2 or H_2 ($C + CO_2 \rightarrow 2CO$, $C + 2H_2 \rightarrow CH_4$) at Ni

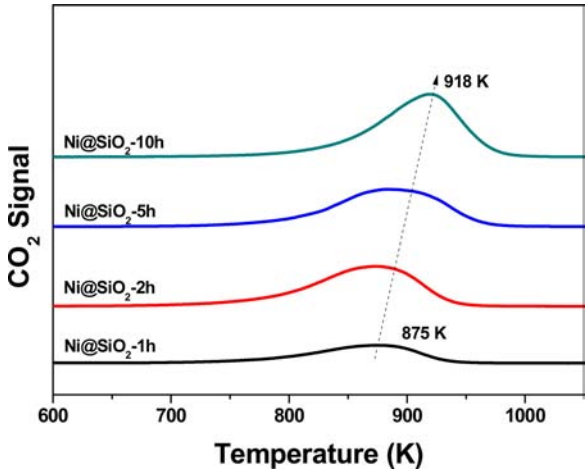

Fig. 10. TPO profiles of the used Ni@SiO_2 catalysts.

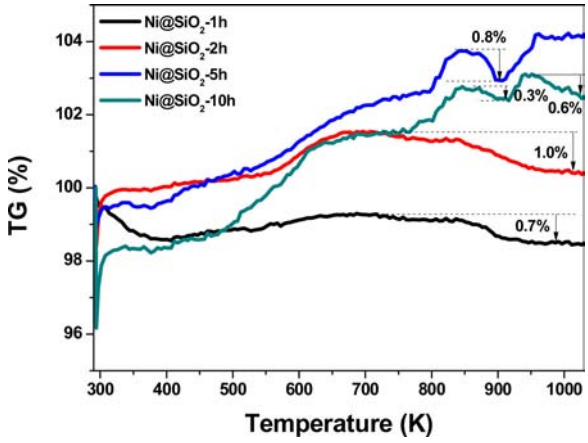

Fig. 11. TG analysis of the used Ni@SiO_2 catalysts after stability tests.

nanoparticle surface or Ni-SiO_2 interface [25]. Because of the relative high activity, catalytic deactivation contribution from the soft carbon deposition was negligible, and therefore resulted in a stable performance (Fig. 7) [15,33].

Although not observed in TEM images, carbon deposits were detected by TPO technique. The result (Fig. 10) shows only one oxidation peak for each used Ni@SiO_2 catalyst, and the peak locations were blue-shifted from the used Ni@SiO_2-1 h catalyst to the used Ni@SiO_2-10 h catalyst. The only one oxidation peak suggested that one type of carbon deposits was produced on the used catalysts. According to literatures [25,29,33,39], carbon deposit oxidation at 800–900 K would be ascribed to amorphous carbon C_α, and the oxidation above 900 K can be assigned to graphitic carbon C_β. From the peak locations in Fig. 10, amorphous carbon should be formed on the used Ni@SiO_2 catalysts. The blue-shift peaks on the other used catalysts might be indicated that the nature of amorphous carbon was different on each used catalysts, or partial amorphous carbon might be transformed to graphitic carbon.

The amount of carbon deposits on the used catalysts were analyzed by TG (Fig. 11). Below 500 K, weight loss should be originated from removal of adsorbed water. Above 500 K, weight increase was observed on the used catalysts. Maximum weight was achieved at 700 K on the used Ni@SiO_2-1 h and Ni@SiO_2-2 h catalysts, followed by a slight weight decrease to 1030 K. The weight increase should be associated with the oxidation of metallic Ni to NiO [33], and the following weight loss could be related with the oxidation of carbon. Total carbon deposits were about 0.7% and 1.0% on the used Ni@SiO_2-1 h and Ni@SiO_2-2 h catalysts, respectively. Besides, the weights were increased to 850 K, and then were slightly decreased at 900 K, on the used Ni@SiO_2-5 h and Ni@SiO_2-10 h catalysts. In the Ni@SiO_2-10 h catalyst, another weight loss peak was observed at around 1020 K. The total carbon deposits were 0.8% and 0.9% on the used Ni@SiO_2-5 h and Ni@SiO_2-10 h catalysts, respectively. The deposits were rather less than those on the Ni catalysts that confined in SiO_2 nanospheres or mesoporous reported by pioneers (1.2 wt% [25], 3.0 wt% [34], 3.6 wt% [20], and 3.8% [43]). The low carbon deposits, although composed fractional composition of graphitic carbon, would not significantly influence performances of the Ni@SiO_2 catalysts [25,39,54].

4. Conclusions

As a summary, we prepared core-shell structured Ni@SiO_2 catalysts that composed of Ni nanoparticles confined in silica shell. The size of Ni nanoparticles was as small as about 5 nm, and the diameter of silica nanospheres was around 30 nm. The Ni@SiO_2 catalysts exhibited excellent stability towards CRM reaction, which was originated from the protection of silica nanospheres that could confine moving spaces of Ni nanoparticles, and the small size of Ni nanoparticles that could lower carbon diffusion in Ni crystals. The former attributed to sintering-free feature and the latter contributed to low carbon deposits. Due to the excellent unique features of sintering-free and low carbon deposits in high temperature CRM, it is believed that the small-sized Ni catalyst could also be applied in many other hydrocarbons catalytic reactions involving sintering and carbon problems.

Acknowledgement

The authors sincerely acknowledge financial supports from National Natural Science Foundation of China (21503142 and 21503113), Jiangsu Province Natural Science Foundation (BK20170526), China Postdoctoral Science Foundation (2017M621644) and Senior Talents Start-Up Fund of Jiangsu University (16JDG062).

Appendix A. Supplementary data

Supplementary material related to this article can be found, in the online version, at doi:https://doi.org/10.1016/j.apcatb.2018.04.069.

References

[1] A.A. Olajire, Valorization of greenhouse carbon dioxide emissions into value-added products by catalytic processes, J. CO2 Util. 3-4 (2013) 74–92.
[2] M. Robert, Running the clock: CO_2 catalysis in the age of anthropocene, ACS Energy Lett. 1 (2016) 281–282.
[3] P. Gao, S. Li, X. Bu, et al., Direct conversion of CO_2 into liquid fuels with high selectivity over a bifunctional catalyst, Nat. Chem. 9 (2017) 1019–1024.
[4] M.D. Porosoff, B. Yan, J.G. Chen, Catalytic reduction of CO_2 by H_2 for synthesis of CO, methanol and hydrocarbons: challenges and opportunities, Energy Environ. Sci. 9 (2016) 62–73.
[5] J. Wei, Q. Ge, R. Yao, et al., Directly converting CO_2 into a gasoline fuel, Nat. Commun. 8 (2017) 15174.
[6] S. Das, J. Ashok, Z. Bian, et al., Silica–Ceria sandwiched Ni core–shell catalyst for low temperature dry reforming of biogas: coke resistance and mechanistic insights, Appl. Catal. B Environ. 230 (2018) 220–236.
[7] R.W. Dorner, D.R. Hardy, F.W. Williams, et al., Heterogeneous catalytic CO_2 conversion to value-added hydrocarbons, Energy Environ. Sci. 3 (2010) 884–890.
[8] L. Zhong, F. Yu, Y. An, et al., Cobalt carbide nanoprisms for direct production of lower olefins from syngas, Nature 538 (2016) 84–87.
[9] X. Li, D. Li, H. Tian, et al., Dry reforming of methane over Ni/La_2O_3 nanorod catalysts with stabilized Ni nanoparticles, Appl. Catal. B Environ. 202 (2017) 683–694.
[10] N. Wang, W. Qian, W. Chu, et al., Crystal-plane effect of nanoscale CeO_2 on the catalytic performance of Ni/CeO_2 catalysts for methane dry reforming, Catal. Sci. Technol. 6 (2016) 3594–3605.
[11] D.H. Kim, J.K. Sim, J. Lee, et al., Carbon dioxide reforming of methane over mesoporous Ni/SiO_2, Fuel 112 (2013) 111–116.
[12] L. Xu, Z. Miao, H. Song, et al., CO_2 reforming of CH_4 over rare earth elements functionalized mesoporous Ni–Ln (Ln = Ce, La, Sm, Pr)–Al–O composite oxides, Int. J. Hydrogen Energy 39 (2014) 3253–3268.
[13] C. Liu, J. Ye, J. Jiang, et al., Progresses in the preparation of coke resistant Ni-based catalyst for steam and CO_2 reforming of methane, ChemCatChem 3 (2011) 529–541.
[14] D. Pakhare, J. Spivey, A review of dry (CO_2) reforming of methane over noble metal

catalysts, Chem. Soc. Rev. 43 (2014) 7813–7837.
[15] C. Wang, N. Sun, N. Zhao, et al., Coking and deactivation of a mesoporous Ni–CaO–ZrO_2 catalyst in dry reforming of methane: a study under different feeding compositions, Fuel 143 (2015) 527–535.
[16] D. Chen, K.O. Christensen, E. Ochoa-Fernández, et al., Synthesis of carbon nanofibers: effects of Ni crystal size during methane decomposition, J. Catal. 229 (2005) 82–96.
[17] N. Abdel Karim Aramouni, J. Zeaiter, W. Kwapinski, et al., Thermodynamic analysis of methane dry reforming: effect of the catalyst particle size on carbon formation, Energy Convers. Manage. 150 (2017) 614–622.
[18] J.W. Han, J.S. Park, M.S. Choi, et al., Uncoupling the size and support effects of Ni catalysts for dry reforming of methane, Appl. Catal. B Environ. 203 (2017) 625–632.
[19] I. Luisetto, S. Tuti, C. Battocchio, et al., Ni/CeO_2–Al_2O_3 catalysts for the dry reforming of methane: the effect of $CeAlO_3$ content and nickel crystallite size on catalytic activity and coke resistance, Appl. Catal. A Gen. 500 (2015) 12–22.
[20] K. Mette, S. Kühl, A. Tarasov, et al., High-Temperature stable Ni nanoparticles for the dry reforming of methane, ACS Catal. 6 (2016) 7238–7248.
[21] T.W. Hansen, A.T. DeLaRiva, S.R. Challa, et al., Sintering of catalytic nanoparticles: particle migration or Ostwald ripening? Acc. Chem. Res. 46 (2013) 1720–1730.
[22] H. Ay, D. Üner, Dry reforming of methane over CeO_2 supported Ni, Co and Ni–Co catalysts, Appl. Catal. B Environ. 179 (2015) 128–138.
[23] M. Usman, W.M.A. Wan Daud, H.F. Abbas, Dry reforming of methane: influence of process parameters-A review, Renew. Sustain. Energy Rev. 45 (2015) 710–744.
[24] I.H. Son, S.J. Lee, I.Y. Song, et al., Study on coke formation over Ni/γ-Al_2O_3, Co-Ni/γ-Al_2O_3, and Mg-Co-Ni/γ-Al_2O_3 catalysts for carbon dioxide reforming of methane, Fuel 136 (2014) 194–200.
[25] J. Zhang, F. Li, Coke-resistant Ni@SiO_2 catalyst for dry reforming of methane, Appl. Catal. B Environ 176–177 (2015) 513–521.
[26] Y. Wang, H. Arandiyan, J. Scott, et al., Recent advances in ordered meso/macroporous metal oxides for heterogeneous catalysis: a review, J. Mater. Chem. A 5 (2017) 8825–8846.
[27] L. Xu, F. Wang, M. Chen, et al., Alkaline-promoted Ni based ordered mesoporous catalysts with enhanced low-temperature catalytic activity toward CO_2 methanation, RSC Adv. 7 (2017) 18199–18210.
[28] X. Du, D. Zhang, R. Gao, et al., Design of modular catalysts derived from NiMgAl-LDH@m-SiO_2 with dual confinement effects for dry reforming of methane, Chem. Commun. 49 (2013) 6770–6772.
[29] W. Yang, H. Liu, Y. Li, et al., Properties of yolk–shell structured Ni@SiO_2 nanocatalyst and its catalytic performance in carbon dioxide reforming of methane to syngas, Catal. Today 259 (2016) 438–445.
[30] X. Feng, W. Li, D. Liu, et al., Self-Assembled Pd@CeO_2/γ-Al_2O_3 catalysts with enhanced activity for catalytic methane combustion, Small 13 (2017) 1700941-n/a.
[31] Z. Li, M. Li, Z. Bian, et al., Design of highly stable and selective core/yolk–shell nanocatalysts-a review, Appl. Catal. B Environ. 188 (2016) 324–341.
[32] H. Tian, X. Li, L. Zeng, et al., Recent advances on the design of group VIII base-metal catalysts with encapsulated structures, ACS Catal. 5 (2015) 4959–4977.
[33] Z. Li, L. Mo, Y. Kathiraser, et al., Yolk–Satellite–Shell structured Ni–Yolk@Ni@SiO_2 nanocomposite-superb catalyst toward methane CO_2 reforming reaction, ACS Catal. 4 (2014) 1526–1536.
[34] Z. Li, Y. Kathiraser, J. Ashok, et al., Simultaneous tuning porosity and basicity of nickel@nickel–magnesium phyllosilicate core–shell catalysts for CO_2 reforming of CH_4, Langmuir 30 (2014) 14694–14705.
[35] T. Wu, W. Cai, P. Zhang, et al., Cu-Ni@SiO_2 alloy nanocomposites for methane dry reforming catalysis, RSC Adv. 3 (2013) 23976–23979.
[36] J.W. Han, C. Kim, J.S. Park, et al., Highly coke-resistant Ni nanoparticle catalysts with minimal sintering in dry reforming of methane, ChemSusChem 7 (2014) 451–456.
[37] U. Cimenler, B. Joseph, J.N. Kuhn, Hydrocarbon steam reforming using Silicalite-1 zeolite encapsulated Ni-based catalyst, AIChE J. 63 (2017) 200–207.
[38] E. Baktash, P. Littlewood, R. Schomäcker, et al., Alumina coated nickel nanoparticles as a highly active catalyst for dry reforming of methane, Appl. Catal. B Environ. 179 (2015) 122–127.
[39] F. Wang, L. Xu, W. Shi, Syngas production from CO_2 reforming with methane over core-shell Ni@SiO_2 catalysts, J. CO2 Util. 16 (2016) 318–327.
[40] B.D. Cullity, Elements of X-ray Diffraction, 2nd ed., Addison-Wesley, Menlo Park, 1978.
[41] L. Li, S. He, Y. Song, et al., Fine-tunable Ni@porous silica core–shell nanocatalysts: synthesis, characterization, and catalytic properties in partial oxidation of methane to syngas, J. Catal. 288 (2012) 54–64.
[42] F. Wang, L. Xu, W. Shi, et al., Thermally stable Ir/$Ce_{0.9}La_{0.1}O_2$ catalyst for high temperature methane dry reforming reaction, Nano Res. 10 (2017) 364–380.
[43] T. Xie, L. Shi, J. Zhang, et al., Immobilizing Ni nanoparticles to mesoporous silica with size and location control via a polyol-assisted route for coking- and sintering-resistant dry reforming of methane, Chem. Commun. 50 (2014) 7250–7253.
[44] P. Ferreira-Aparicio, A. Guerrero-Ruiz, I. Rodríguez-Ramos, Comparative study at low and medium reaction temperatures of syngas production by methane reforming with carbon dioxide over silica and alumina supported catalysts, Appl. Catal. A Gen. 170 (1998) 177–187.
[45] U. Oemar, Y. Kathiraser, L. Mo, et al., CO_2 reforming of methane over highly active La-promoted Ni supported on SBA-15 catalysts: mechanism and kinetic modelling, Catal. Sci. Technol. 6 (2016) 1173–1186.
[46] R.Y. Chein, W.H. Hsu, C.T. Yu, Parametric study of catalytic dry reforming of methane for syngas production at elevated pressures, Int. J. Hydrogen Energy 42 (2017) 14485–14500.
[47] H. Atashi, J. Gholizadeh, F. Farshchi Tabrizi, et al., Thermodynamic analysis of carbon dioxide reforming of methane to syngas with statistical methods, Int. J. Hydrogen Energy 42 (2017) 5464–5471.
[48] B. Abdullah, N.A. Abd Ghani, D.-V.N. Vo, Recent advances in dry reforming of methane over Ni-based catalysts, J. Clean. Prod. 162 (2017) 170–185.
[49] L. Xu, F. Wang, M. Chen, et al., Alkaline-promoted Co-Ni bimetal ordered mesoporous catalysts with enhanced coke-resistant performance toward CO_2 reforming of CH_4, J. CO2 Util. 18 (2017) 1–14.
[50] J.L. Pinilla, I. Suelves, M.J. Lázaro, et al., Influence of nickel crystal domain size on the behaviour of Ni and NiCu catalysts for the methane decomposition reaction, Appl. Catal. A Gen. 363 (2009) 199–207.
[51] L.C.S. Kahle, T. Roussière, L. Maier, et al., Methane dry reforming at High temperature and elevated pressure: impact of gas-phase reactions, Ind. Eng. Chem. Res. 52 (2013) 11920–11930.
[52] O. Omoregbe, H.T. Danh, C. Nguyen-Huy, et al., Syngas production from methane dry reforming over Ni/SBA-15 catalyst: effect of operating parameters, Int. J. Hydrogen Energy 42 (2017) 11283–11294.
[53] M.M. Nair, S. Kaliaguine, F. Kleitz, Nanocast $LaNiO_3$ perovskites as precursors for the preparation of coke-resistant dry reforming catalysts, ACS Catal. 4 (2014) 3837–3846.
[54] C.H. Bartholomew, Mechanisms of catalyst deactivation, Appl. Catal. A Gen. 212 (2001) 17–60.
[55] J. Wei, E. Iglesia, Isotopic and kinetic assessment of the mechanism of reactions of CH_4 with CO_2 or H_2O to form synthesis gas and carbon on nickel catalysts, J. Catal. 224 (2004) 370–383.
[56] W. Li, Z. Zhao, G. Wang, Modulating morphology and textural properties of ZrO_2 for supported Ni catalysts toward dry reforming of methane, AIChE J. 63 (2017) 2900–2915.
[57] Z. Zhang, X.E. Verykios, Carbon dioxide reforming of methane to synthesis gas over Ni/La_2O_3 catalysts, Appl. Catal. A Gen. 138 (1996) 109–133.